JOURNAL OF MATERIALS SCIENCE 35 (2000) 3415–3423

Effect of water vapor on the mechanical behaviors of hot isostatically pressed silicon nitride containing Y_2O_3

HONGSANG RHO, N. L. HECHT*, G. A. GRAVES
University of Dayton Research Institute, Dayton, Ohio 45469-0172, USA
E-mail: jhecht@flyernet.udayton.edu

The effect of water vapor on the mechanical behavior of Si_3N_4 ceramics was studied. Strength measurements by flexural dynamic fatigue tests were made at temperatures from 1038°C to 1350°C and at actuator speeds of 8.4×10^{-2} and 8.4×10^{-5} mm/s (~200 and ~0.2 MPa/s). Step stress rupture tests were also performed at 1288°C and 1150°C. Water vapor had a beneficial effect on the flexural strength due to flaw healing, and/or blunting mechanisms. Dynamic fatigue results demonstrated that the beneficial effects of water vapor on the strength increases as temperature increases and/or loading rate decreases. Time-to-failure was always longer in wet air during step stress rupture testing. Creep crack growth by formation and coalescence of cavities ahead of the crack tip generated from the oxidation pits or subsurface pores were the primary mechanism for slow crack growth for NT 164 Si_3N_4.

1. Introduction

Only limited investigations have been conducted on the effect of water vapor in the oxidation process of silicon based polycrystalline ceramics [1–3]. Furthermore, in a search of the literature no reference was found to work investigating only the effect of water vapor on the long-term mechanical properties of Si_3N_4 ceramics. If polycrystalline Si_3N_4 is to be used in heat exchangers, gas turbines etc., it is essential to understand how water vapor affects the oxidation behavior and how it interacts with the mechanical behavior of these materials. To investigate the effect of water on the mechanical behavior, dynamic fatigue tests and step stress rupture tests were performed on a commercial Si_3N_4–4 w% Y_2O_3 manufactured 1995 by Norton company, designated NT-165-95.

2. Experimental procedure

2.1. Materials

NT 164-95 test bars (Si_3N_4 containing 4 w% Y_2O_3 sintering aid, 1995 vintage) were used for both the dynamic fatigue tests and the stress rupture tests.

2.2. Dynamic fatigue tests

Dynamic fatigue testing of type B flexural bars ($3 \times 4 \times 50$ mm) were conducted following ASTM-C1211-92 in both air and wet air using a SiC four-point bend fixture in a universal testing machine (Instron Universal Testing Machine 5500R123, Instron Corp., Canton, MA). The universal testing machine is equipped with a $MoSi_2$ heated furnace. The inner and outer spans were 20 and 40 mm, respectively. Two different crosshead speeds, 8.4×10^{-2} and 8.4×10^{-5} mm/s, were used to determine susceptibility to slow crack growth at three different temperaures, 1038, 1150, and 1350°C. Ten specimens were tested at each of the test conditions.

Fig. 1 shows a schematic diagram of the apparatus used for the dynamic fatigue tests and step stress rupture tests in air with 6.4 vol% H_2O. The water content was obtained by bubbling air through deionized water in three flasks immersed in an isothermal bath. The dew point was measured by a hygrometer midway between the isothermal water bath and the furnace. The desired dew point (6.4 vol% H_2O) was obtained by controlling the water temperature in the isothermal water bath. The temperature variation in the dew point was controlled to within 0.5°C with this system. A polymer tube was used in the water generating system and converted to a stainless steel tube to the furnace. The temperature inside the polymer tube was kept at 65°C and the temperature inside the stainless tube was kept at 150°C to prevent the water vapor in the air stream from condensing and preheating the air before entering into the furnace. The effects of increased levels of water vapor on the flexural strength were determined by enclosing the test bars in a porcelain chamber in the furnace and introducing controlled amounts of water vapor during testing. Air containing 6.4 vol% of water vapor was piped into the furnace 25 minutes

* Author to whom all correspondence should be addressed.

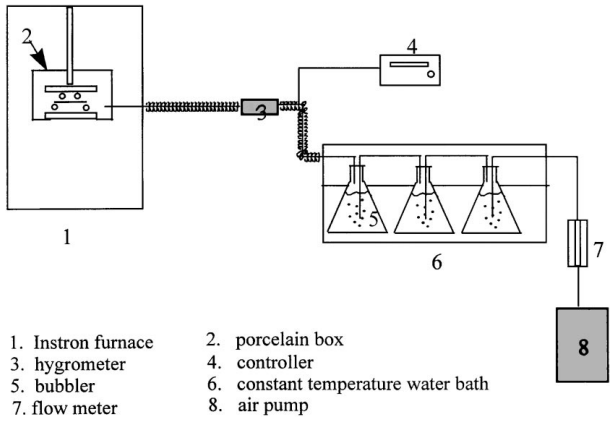

Figure 1 Schematic diagram of the water generating system in the dynamic fatigue testing.

TABLE I Schedule of step stress rupture tests for NT 164-95

1150°C	Time	8 hours →	48 hours →	24 hours
	Stress[a]	1/2 σ	3/4 σ	9/10 σ
1288°C	Time	8 hours →	48 hours →	24 hours
	Stress[a]	1/2 σ	3/4 σ	9/10 σ

[a]σ is 628 MPa.

before reaching the target temperature. The heating rate was 100°C/min. After 10 minutes of reaching the target temperature, the testing stress was applied, which allowed the system to thermally equilibrate.

2.3. Step stress rupture tests

Step stress rupture testing was conducted in a SiC glow bar furnace. The specimens were loaded in four point bend SiC fixtures. The inner and outer span were 20 and 40 mm, respectively. Stress was applied using a deadweight cantilever system. The furnace were heated to the target temperature under a small load and stabilized for 2 hours at the target temperature. Heating of the furnace was achieved with a set point controller. The stress was applied and increased according to a predefined schedule. If the specimen survived to the end of the step loading schedule, the retained strength was measured at the selected test temperature. If the specimen was broken during the step loading test, the time to failure was recorded. The step stress schedule for NT 164-95 is presented in Table I.

2.4. Analysis

An optical microscope (OM, Nikon Epiphot, Nikon Co., Japan) was used to determine the general location of the fracture origins of the mechanically tested specimens. Higher magnification observations of the failure origin were performed with a scanning electron microscope (SEM). To prevent charging on the specimens, a carbon coating was used to examine the morphology and to conduct the elemental analysis. A Gold-Palladium coating was used only for the topographical analysis.

3. Results and discussions

3.1. Dynamic fatigue tests

The results of the flexural strength measurement for investigation of the dynamic fatigue behavior of NT 164-95 are summarized in Table II. Between 1038 and 1350°C the strength measured at the rapid stressing rate dropped 15% with increasing temperatures. The drop of strength as a function of temperature is an indication of the sensitivity of the grain boundary phase to temperature change. The drop in strength as a function of temperature is dependent on the amount and viscosity of the grain boundary glass phase. The greater the amount of glass phase and its higher sensitivity to viscosity, the greater the strength drop observed. Weibull plots of the flexural strength data for NT 164 were prepared (see Figs 2 and 3) in an effort to identify behavioral trends. Fracture origins varied with environments and test conditions. These fractures tended to originate at machining defects, processing defects or pits that were generated during exposure to oxidation conditions. NT 164 demonstrated a distinctive bimodal statistical strength. Table III shows the Weibull flexural strength characterization of NT 164. In most cases, the strength recorded for volume failures was lower than those recorded for surface failure. The data for volume failure strengths were also more scattered. All specimen failures at 1350°C and at a stressing rate of 0.0002 in/min, except one, originated from the corner.

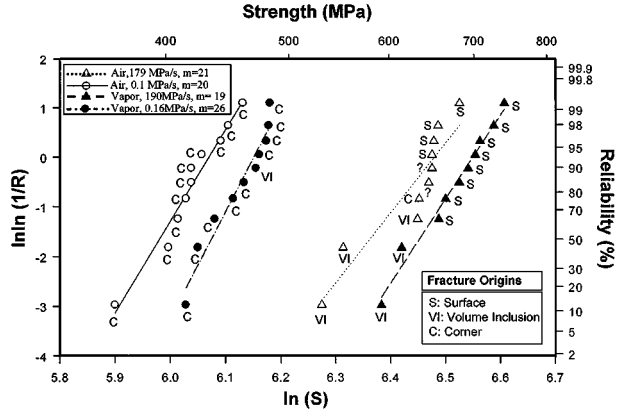

Figure 2 Weibull plot comparison of flexural strength of NT 164 in air and in wet air (6.4 Vol%) at 1350°C.

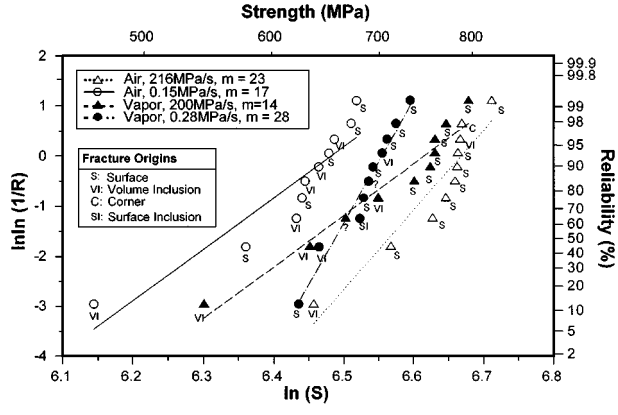

Figure 3 Weibull plot comparison of flexural strength of NT 164 in air and in wet air (6.4 Vol%) at 1150°C.

TABLE II Summary of Dynamic Fatigue Test Results of NT 164 in Air and Wet air

EMP (°C)	ATM	Stressing rate (MPa/S)	SCG exponent (n)	Average strength (MPa)	STD. dev. (MPa)	Weibull (m)	Fracture origin[a]
1350	Air	180	18	628	48	21	4 surf, 3 vol. inc., 2?, 1 edge
	Air	0.1		421	27	20	SCG from edge
	Wet air	190	18	678	47	19	5 surf, 3 vol. inc., 2?
	Wet air	0.16		457	25	26	9 edge, 1 surf
1150	Air	215	35	761	52	23	7 surf, 2 vol. inc., 1 edge
	Air	0.15		622	62	17	5 surf, 5 vol. inc.
	Wet air	200	191	711	77	14	6 surf, 3 vol. inc., 1?
	Wet air	0.3		688	33	28	7 surf (1 Inc.), 2 vol. inc., 1?
1038	Air	153	159	737	89	15	6 surf, 3 vol. inc., 1?
	Air	0.16		706	42	25	8 surf, 1 edge inc., 1?

[a]Surf: surface
Vol. Inc.: volume inclusion
?: unknown
Temp: Temperature
ATM: Atmosphere
SCG exponent: Slow crack growth exponent
STD. DEV.: Standard deviation
Wet air: air + 6.4 vol% H_2O

TABLE III NT 164 Weibull flexural strength characterization

loading rate $= 8.4 \times 10^{-2}$ mm/s	1150°C, air	1150°C, wet air	1350°C, air	1350°C, wet air
Average strength, surface	772 Mpa	762 Mpa	659 Mpa	693 Mpa
Standard deviation	(45)	(36)	(33)	(40)
Average strength, volume	711 Mpa	626 Mpa	571 Mpa	603 Mpa
Standard deviation	(111.2)	(83)	(61)	(38)
Weibull modulus, surface	28	45	41	29
Weibull modulus, volume	8	9	12	—
Weibull scale factor, surface	187	298	268	189
Weibull scale factor, volume	50	59	74	—
loading rate $= 8.4 \times 10^{-5}$ mm/s				
Average strength, surface	641 Mpa	692 Mpa		
Standard deviation	(49)	(45)		
Average strength, volume	603 Mpa	677		
Standard deviation	(83)	(45)		
Weibull modulus, surface	18	23		
Weibull modulus, volume	7	24		
Weibull scale factor, surface	118	149		
Weibull scale factor, volume	48	159		

Fig. 4 shows (a) a typical corner failure for NT 164 at 1350°C and (b) an inclusion failure. These corner failures were attributed to the formation of new flaws which appeared to be a porous layer beneath the oxide layer. The inclusion in Fig. 4b was found by EDX to be rich in Fe, K, and Na. The K and Na contamination was attributed to the glass encapsulation used during fabrication. For the NT 164 specimens tested in air and wet air at 1350°C at the rapid stressing rate (0.2 in/min), 30% failed by volume originated flaws. When the test temperature was decreased to 1150°C, the percent of volume failures at the rapid stressing rate (0.2 in/min) was 30% in wet air and 20% in air. However, the number of volume failures in air increaed at the slower stressing rate (0.0002 in/min), but decreased in wet air. The percent of volume failures was 50% (air) and 20% (wet air). Fig. 5 is an SEM fractograph showing a typical volume initiated failure in a specimen tested at 1150°C. The inclusion was found to be rich in Fe and Ni. Residual stresses develop around the inclusion due to the thermal expansion coefficient and the elastic constant differences between the matrix and the inclusion. Fe-Ni inclusions have higher thermal contraction and lower elastic modulus than the matrix, which induces radial crack around the equatorial position of the inclusion [4]. Fe ions also tend to increase grain growth during sintering since it decreases the viscosity of the liquid phase at the sintering temperature. The decreased percentage of failure initiations at fabrication flaws as the test temperature is increased at slow stressing rates indicates a tendency for inherent flaws to become less competitive with new flaws at the corner by crack blunting of inherent flaws, as described by Menon *et al*. [5].

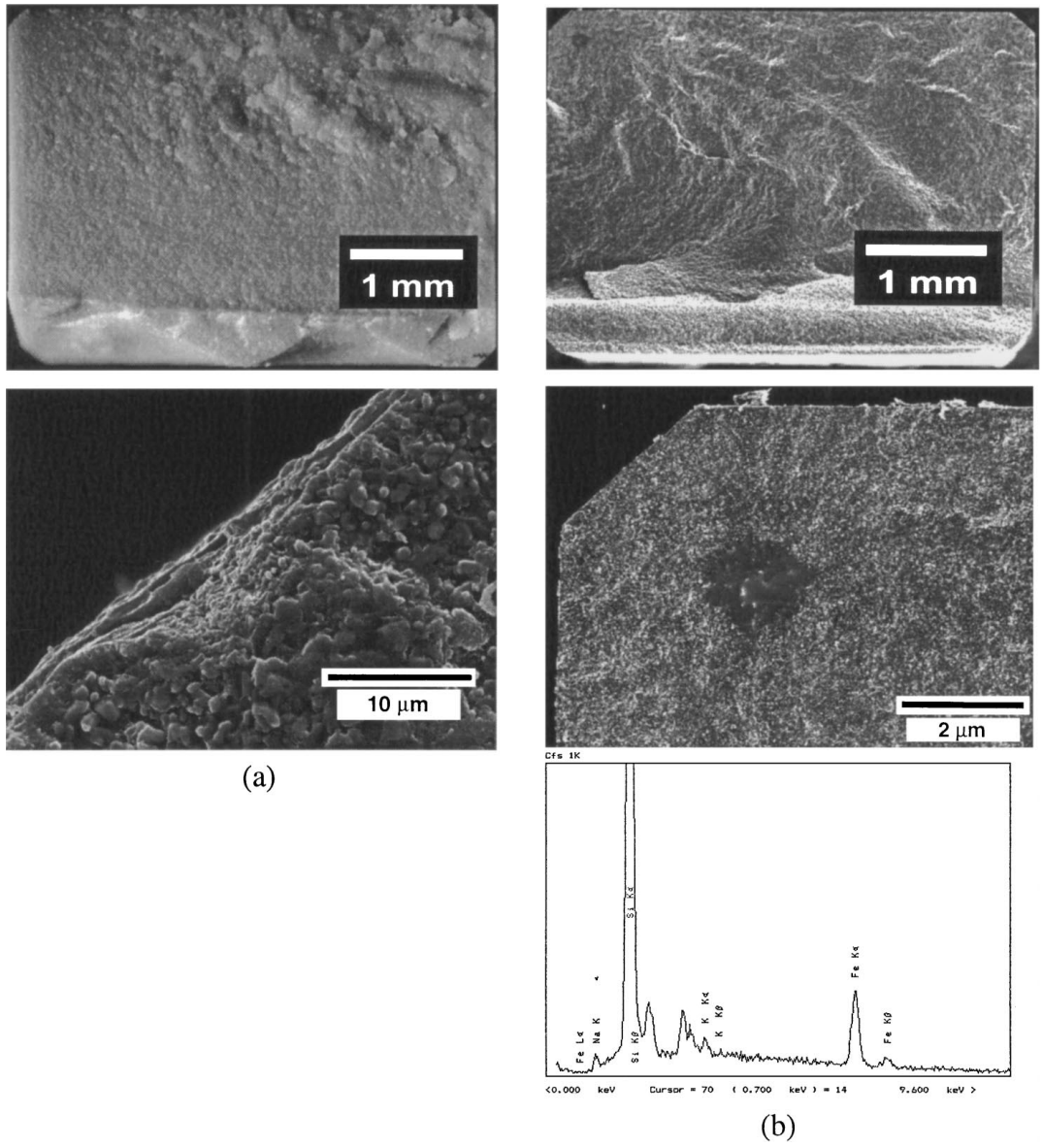

Figure 4 Fracture origins of NT 164: (a) typical corner failure and (b) inclusion failure and EDX of the inclusion.

The slow crack growth coefficients were found to be 18 at 1350°C, 35 at 1150°C and 159 at 1038°C in air and 18 at 1350°C and 191 at 1150°C in wet air suggesting the likelihood for slow crack growth at 1350°C and 1150°C. The flexural strength in the presence of water vapor is higher than the strength measured in air at 1350°C for both stressing rates. At 1150°C the flexural strength in air was higher than the stress measured in the presence of water vapor at the rapid stressing rate, however, at the slow stressing rate the strength in the presence of water vapor is higher than the strength measured in air. Since only the surface failures are affected by environment, one possible strengthening effect by the presence of water is healing of surface flaws such as machining flaws and flaws generated during stressing (new flaws). Another possible reason for higher strength in wet air than in air at the slow loading rate is blunting at the crack tip by the interaction with water vapor.

3.2. Stress rupture tests

Step stress rupture tests were conducted on sixteen B-size NT 164-95 flexure specimens; 8 specimens at 1150°C and 8 specimens at 1288°C. At each temperature 4 specimens were tested in air and 4 specimens were tested in wet air. In the first 8 hours, the NT 164 specimens were loaded to 314 MPa. If the specimens survived, the applied stress was increased to 471 MPa for 48 hours. The applied stress was increased to 571 MPa for another 24 hours for those specimens that survived the 48 hours at the 471 MPa stress level. The specimens that did not break during the entire step stress schedule were subsequently loaded to failure.

The results of the NT164 step stress rupture tests are plotted in Fig. 6. One specimen survived the entire test schedule in each condition (air and wet air). Their average retained strength was 805 MPa which is about 100 MPa higher than the average fast fracture strength. Time to failure was higher in wet air compared to air at both test temperatures (1150°C and 1288°C). It was observed from the statistical analysis that only a small overlap occurs at the 95% confidence level for the two conditions. The scatter in the data was reduced as temperature increased from 1150°C to 1288°C. This reduction in scatter as a function of temperature was also observed for hot pressed Si_3N_4 by Quinn *et al*.

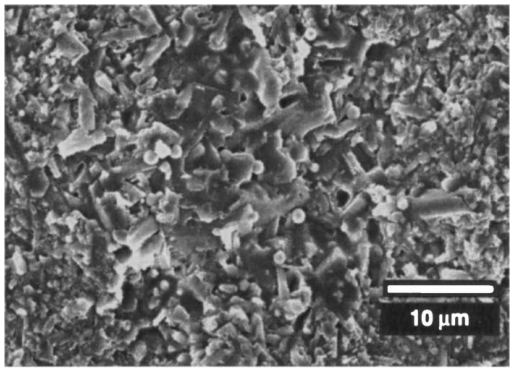

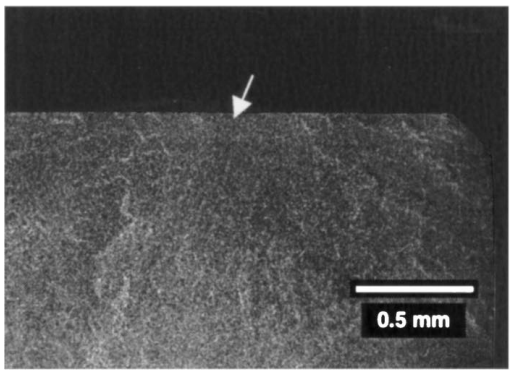

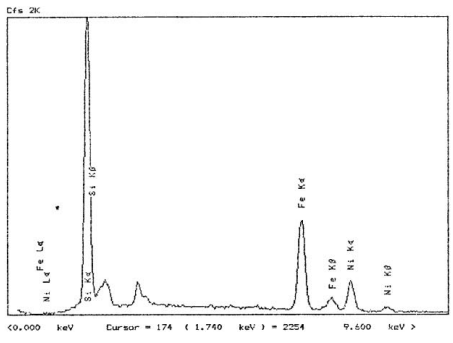

Figure 5 Typical inclusion failures of NT 164 at 1150°C.

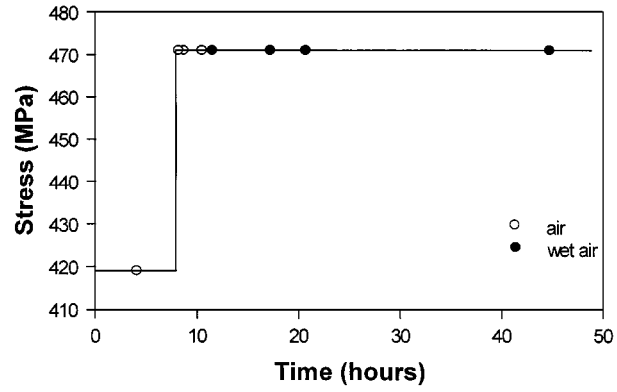

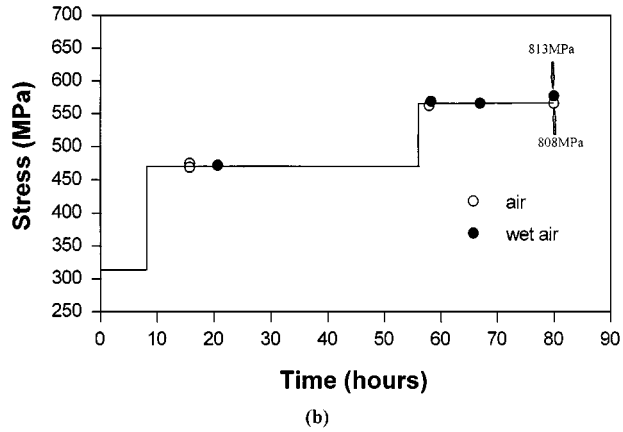

Figure 6 The results of step stress rupture tests of NT 164 at (a) 1288°C and (b) 1150°C.

[6, 7]. Wider scatter of data at lower temperature can be explained by concepts developed by Wiederhorn [8]. If slow crack growth, new flaw generation, and crack healing occurs simultaneously, it will change the appearance of the strength diagram for time invariant distribution. Wiederhorn [8] stated that "Strength enhancement will occur for initial strengths that are greater than the fatigue limit, whereas strength degradation will occur for initial strengths that are below the fatigue limit." In this study, the mechanisms of strength enhancement were crack healing and stress relaxation due to the difference in creep rate between the compression and tension zones of the test specimen. Strength degradation mechanisms were cavitation, crack growth and the generation of new flaws, such as oxidation pitting and porous layer formation below the oxide layer. For the specimens which have strengths close to the fatigue limit, crack growth will be slow, however, crack growth will be fast for the specimens which have strengths that lie close to the applied stress. The two mechanisms for strength degradation and strength enhancement compete with each other over time at stress. Uniform flaw healing and narrow distribution of new flaws seemed to be more dominant as the temperature increased from 1150°C to 1288°C. This effect causes the smaller data scatter at 1288°C. In addition, the strengthening effect was more evident in wet air than in air.

It is interesting to note that fracture origins at 1150°C at stressing rates of 0.5 MPa/s (air) and 0.3 MPa/s (wet air) in the dynamic fatigue tests were predominantly from surface and volume inclusions. Fracture origins in the step stress rupture tests were predominantly at the corners (except for two specimen which failed at an oxidation pit on the surface and at a volume inclusion). These results show that different failure mechanisms intervene during the extended exposure under stress. Typical fracture surfaces are presented in Fig. 7. Crack blunting around inclusions and flaw healing of machining flaws results in the inherent flaws becoming less competitive with new flaw generation [9]. EDX shows the area around the oxidation pit to be rich in Na and Al ions, which would associate with contamination from the glass encapsulation and the environment. Fig. 8 shows the beveled surface of the test specimen etched with HF solution for a few minutes. Compared to the unstressed region, a high density of oxidation pits and worm-like porous arrays (micropores) are observed in the stressed region, which formed under the oxide layer. At the fracture origin, oxidation pitting was observed in the NT 164 stress ruptured specimens at both 1150 and 1288°C. Slow crack growth seems to start from new flaws such as oxidation pits or micropores.

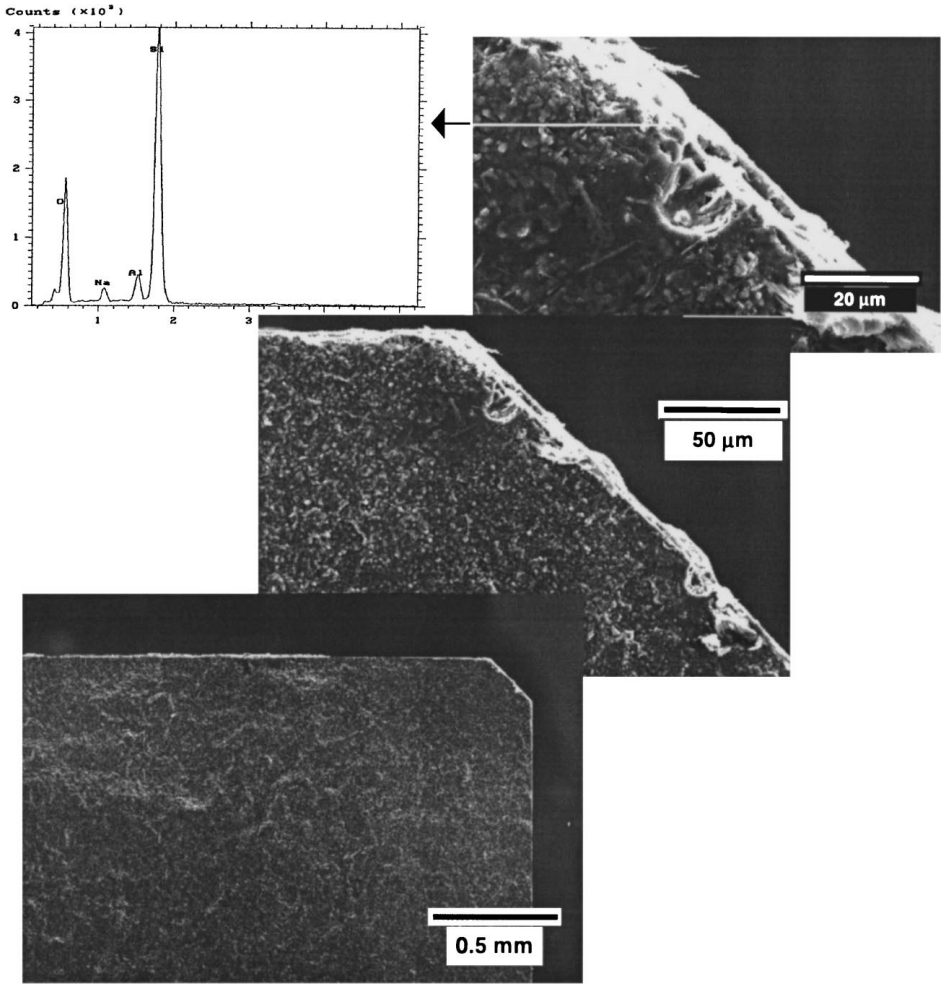

Figure 7 Typical corner failure of NT 164.

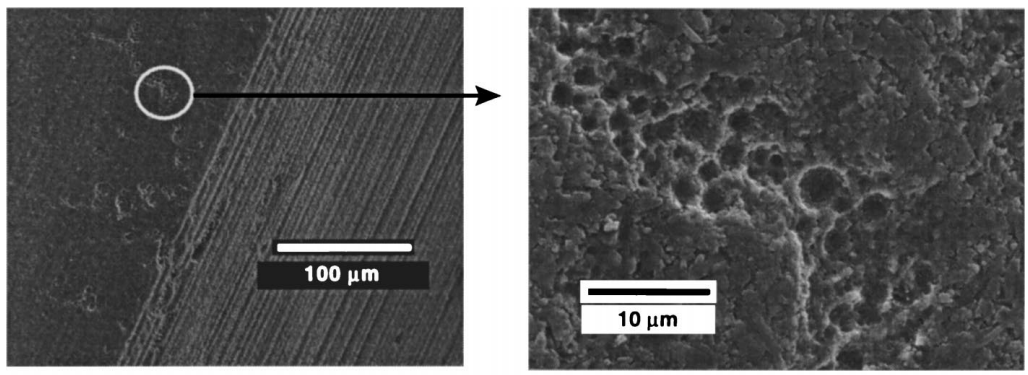

(a) stressed zone

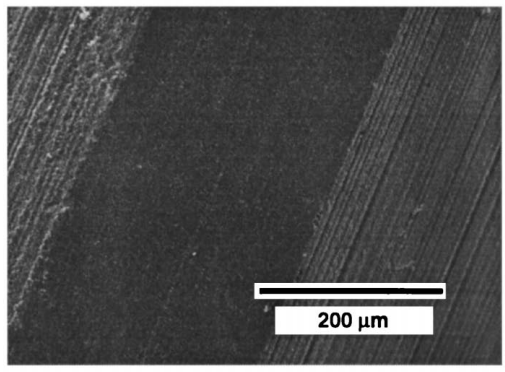

(b) non-stressed zone

Figure 8 Comparison of morphologies between stressed corner and non-stressed corner of NT 164 stress ruptured at 1288°C in air.

The crack propagation process is discussed in a subsequent part of this section.

The permanent deformation curvature of stress ruptured specimen was determined by measuring the curvature of broken specimens. Curvature was determined by scanning along the center 10 mm within the inner loading span with a profilometer according to the method developed by Jakus and Wiederhorn [10]. If this area was not available, the scanning procedure was performed on the area as far as possible from the loading points because of the anomalies which exist at the loading points. The curvature of a test specimen has the following correlation with beam deflection [10]:

$$\frac{1}{\rho} = \frac{d^2y/dx^2}{[1 + (dy/dx)^2]^{3/2}} \quad (1)$$

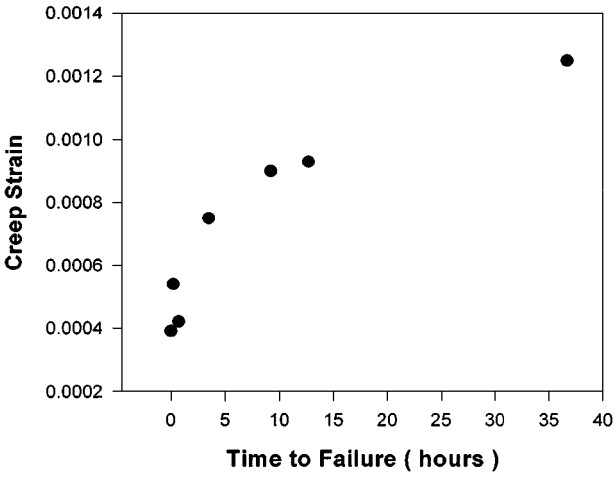

Figure 9 Permanent strain as a function of time-to-failure for NT 164 from stress rupture tests at 1288°C.

where $1/\rho$ is the curvature, y is the beam deflection, and x is the distance along the beam. Since beam deflection for the ceramic materials is quite small, first derivative can be neglected. Creep strain of NT 164 was dependent on the temperature, stress and failure time. The creep failure strain increased as the test temperature increased from 1150°C ($\varepsilon = 0.00012$ to 0.00041) to 1288°C ($\varepsilon = 0.00040$ to 0.00125). The Monkman-Grant model for Si_3N_4 ceramics adequately describes a power-law relation between the minimum creep rate at the constant stress and temperature, i.e.

$$t_f = K(\dot{\varepsilon}_s)^{b_1} \quad (2)$$

where, K and b_1 are constants. Raj [11] demonstrated that the cumulative data of Monkman-Grant relations for Si_3N_4, on the average, fit the inverse linear form of Equation 2, i.e. $b_1 = 1$. Therefore, accumulated strain (ε_f) should be constant or increases moderately as a function of rupture time if failure is strain dependent. The relation between creep strain and t_f of NT 164 at 1288°C is plotted in Fig. 9. Creep strain increased as a function of t_f in a parabolic manner. Menon *et al.* [12] obtained this relation at the low temperature for which slow crack growth is predominent and also explained that the deviation of b_1 from -1 are from crack blunting. From this plot, it is concluded that the fracture was not controlled by creep strain. This fact supports the observance that fracture of NT 164 was due to slow crack growth. Usually, the high deformation resistance of the matrix phase results in non-uniform cavity growth. Cavities on the two grain interfaces were not observed in the broken samples. The only distinct cavities observed are ahead of the crack tip. Fig. 10 shows the secondary crack profiles for the side of a stress ruptured NT 164 specimens. At high temperature (1288°C) crack

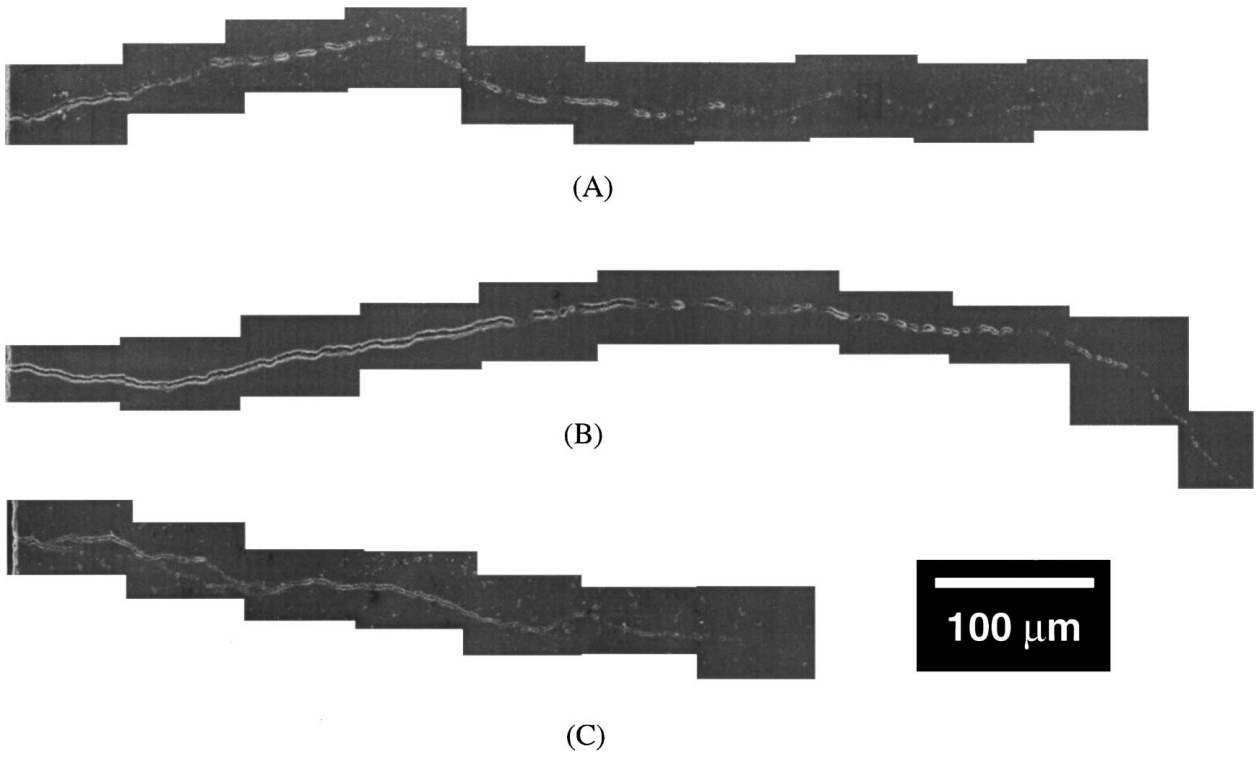

Figure 10 Crack profiles of NT 164 specimens stress ruptured at (a) 1150°C, air, (b) 1150°C, wet air (c) 1288°C, wet air.

branching is frequent, while minimal crack branching is observed at low temperature. A larger damage generation zone is formed at low temperature than at high temperature where damage zones can be readily connected. This damage generation zone is much larger in air than in wet air. Since less than four secondary cracks were observed in the inner loading sections of a NT 164 specimens that failed at 1150 and 1288°C, the cracks must grow to a critical size in a relatively short time if cavity coalescence starts. The largest fraction of time to failure is for the formation and nucleation of cracks (stress concentrators) and the formation of cavities. New flaws which act as stress concentrators can be oxidation pits or micropores. Cavities nucleate and grow until they reach full facet size, and coalescence. Enhanced self healing of new flaws by the higher content of water vapor seems to delay the growth of new flaws and prevent cavity nucleation. A greater numbers of microcracks are observed in the specimens tested in wet air than in air. Raj [13] has described interactive mechanisms with the environment, where cavities form in a local zone of damage near the crack tip and

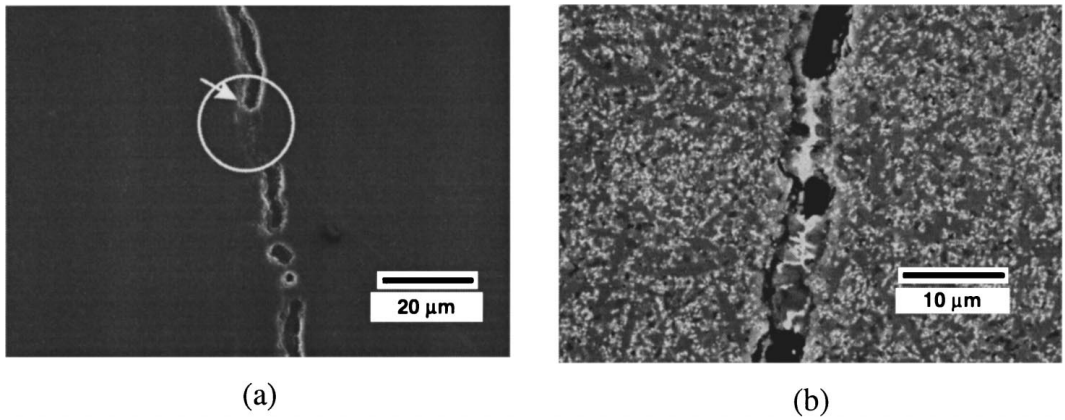

Figure 11 SEM photos of (a) the crack tip of NT 164 specimen stress ruptured at 1150°C (b) stretched glassy phase in front of the crack tip marked by the circle in (a).

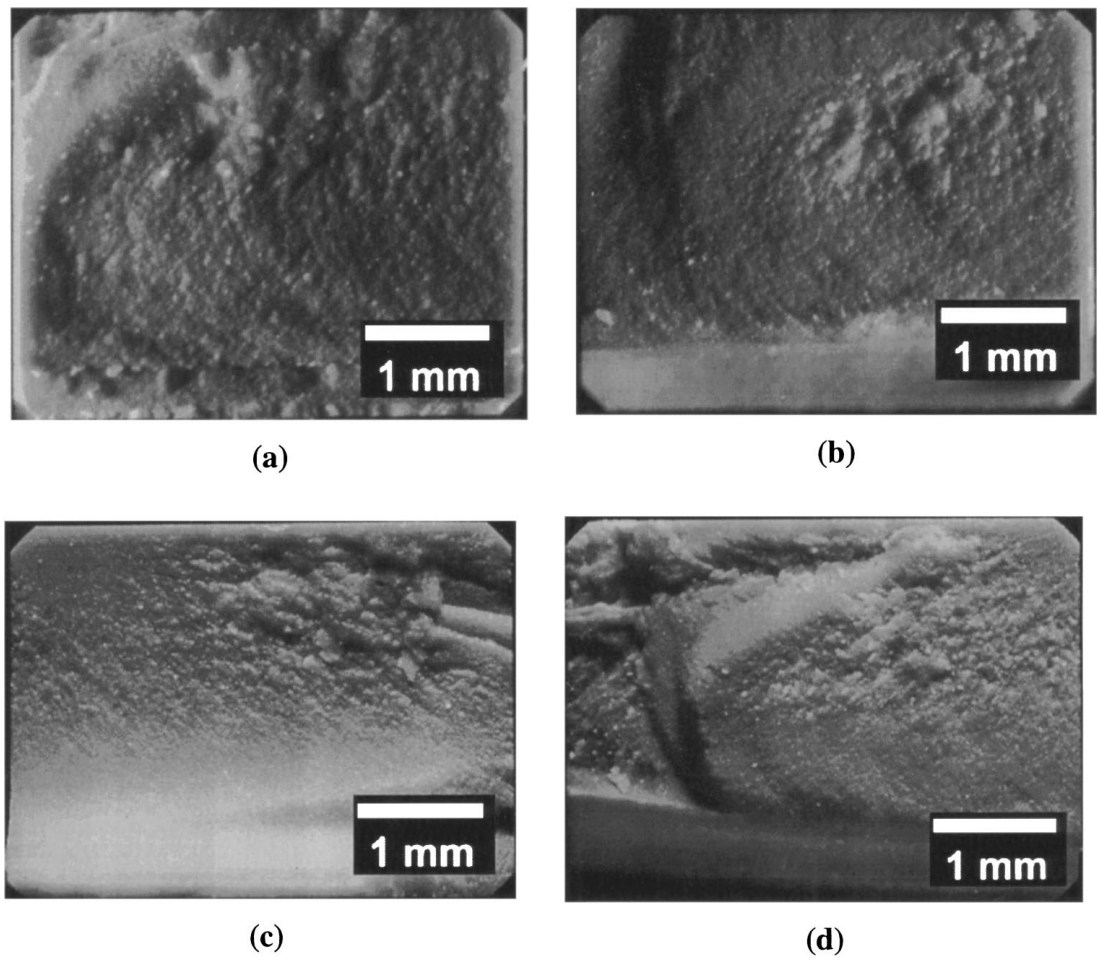

Figure 12 Optical fractography of stress ruptured NT 164 specimens: (a) 1150°C in air, (b) 1150°C in wet air, (c) 1288°C in wet air, and (d) 1288°C in air (preoxidized specimen fractured during loading).

promote crack propagation. To separate the effect of environmental interactive mechanisms on crack propagation from the effect of environment on flaw or crack healing will require more sophisticated research. Crack growth rate measurement as a function of stress intensity for a double cantilever or double torsion specimens may be one possible way to further investigate these interactive mechanisms on crack propagation, such as the effect of internal oxidation on cavitation or stress corrosion cracking. A sharper crack tip is observed at the higher temperature. A stretched glassy phase in the ligand below the crack tip is also observed (Fig. 11). From this observation, it is recognized that the slow crack growth of NT 164 in the step stress rupture test is caused by localized cavitation and damage is connected by stretching of the glassy phase in the ligand.

Fig. 12 shows optical microscope photographs of fracture surfaces for the specimens tested at 1150 and 1288°C in air and wet air. Slow crack growth regions are not quite certain, but seems to be located within mirror like regions. The size of these slow crack growth regions increased at the higher test temperatures and in wet air vs. air. The specimen which fractured during increased loading (Fig. 12d) has a small smooth zone because there is not enough time for slow crack growth.

4. Summary of findings

The major results of the mechanical behavior studied can be summarized as follows;

1) NT 164 shows a distinct bimodal strength distribution in dynamic fatigue testing.

2) Water vapor increases the strength of NT 164 ceramics because of flaw healing or crack blunting.

3) Time to failure in the stress rupture tests was always greater in wet air for NT 164.

4) The scatter in the step stress rupture data of NT 164 is reduced as temperature was increased from 1150°C to 1288°C.

5) The failure mechanism found for NT 164 in the step stress rupture tests was slow crack growth from new flaws.

6) Creep crack growth by formation and coalescence of cavities with stress corrosion cracking ahead of the crack tip from oxidation generated pits or subsurface pores was the primary mechanism for slow crack growth of NT 164.

References

1. M. MAEDA, K. NAKAMURA and T. OHKUBO, *J. Mater. Sci*. **23** (1988) 3933.
2. *Idem*., *ibid*. **24** (1989) 2120.
3. K. KOMEYA, Y. HARUNA, T. MEGURO, T. KAMEDA and M. ASAYAMA, *ibid*. **27** (1992) 5727.
4. J. P. SINGH, *Advanced Ceramic Materials* **3**(1) (1988) 18.
5. M. N. MENON, H. T. FANG, D. C. WU, M. G. JENKINS and M. K. FERBER, *J. Amer. Ceram. Soc*. **77**(5) (1994) 1235.
6. G. D. QUINN, *J. Mater. Sci*. **25** (1990) 4361.
7. G. D. QUINN and J. B. QUINN, in "Fracture Mechanics of Ceramics, Vol. 6," edited by R. C. Bradt, D. P. H. Hasselman and F. F. Lange (Plenum Press, New York, 1978).
8. S. M. WIEDERHORN, in "Fracture Mechanics of Ceramics, Vol. 5: Surface Flaws, Statistics and Microcracking," edited by R. C. Bradt, A. G. Evans, D. P. H. Hasselman and F. F. Lange (1983) p. 197.
9. M. N. MENON, H. T. FANG, D. C. WU, M. G. JENKINS and M. K. FERBER, *J. Amer. Ceram. Soc*. **77**(5) (1994) 1235.
10. JAKUS and S. M. WIEDERHORN, *ibid*. **71**(10) (1988) 832.
11. R. RAJ, *ibid*. **76**(9) (1993) 2147.
12. M. N. MENON, H. T. FANG, D. C. WU, M. G. JENKINS, M. K. FERBER, K. L. MORE, C. R. HUBBARD and T. A. NOLAN, *ibid*. **77**(5) (1994) 1217.
13. R. RAJ, *ibid*. **76**(9) (1993) 2147.

Received 23 February
and accepted 17 November 1999